

12

DAVID W. TAYLOR NAVAL SHIP
RESEARCH AND DEVELOPMENT CENTER

Bethesda, Maryland 20084



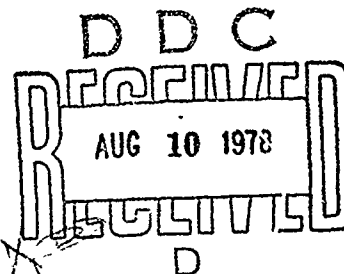
POWERING PREDICTION FOR SURFACE EFFECT SHIPS
BASED ON MODEL RESULTS

by

R. A. Wilson
S. M. Wells
C. E. Heber

APPROVED FOR PUBLIC RELEASE: DISTRIBUTION UNLIMITED

Reprinted from AIAA Paper 78-744



AVIATION AND SURFACE EFFECTS DEPARTMENT
RESEARCH AND DEVELOPMENT REPORT

July 1978

DTNSRDC-78/062

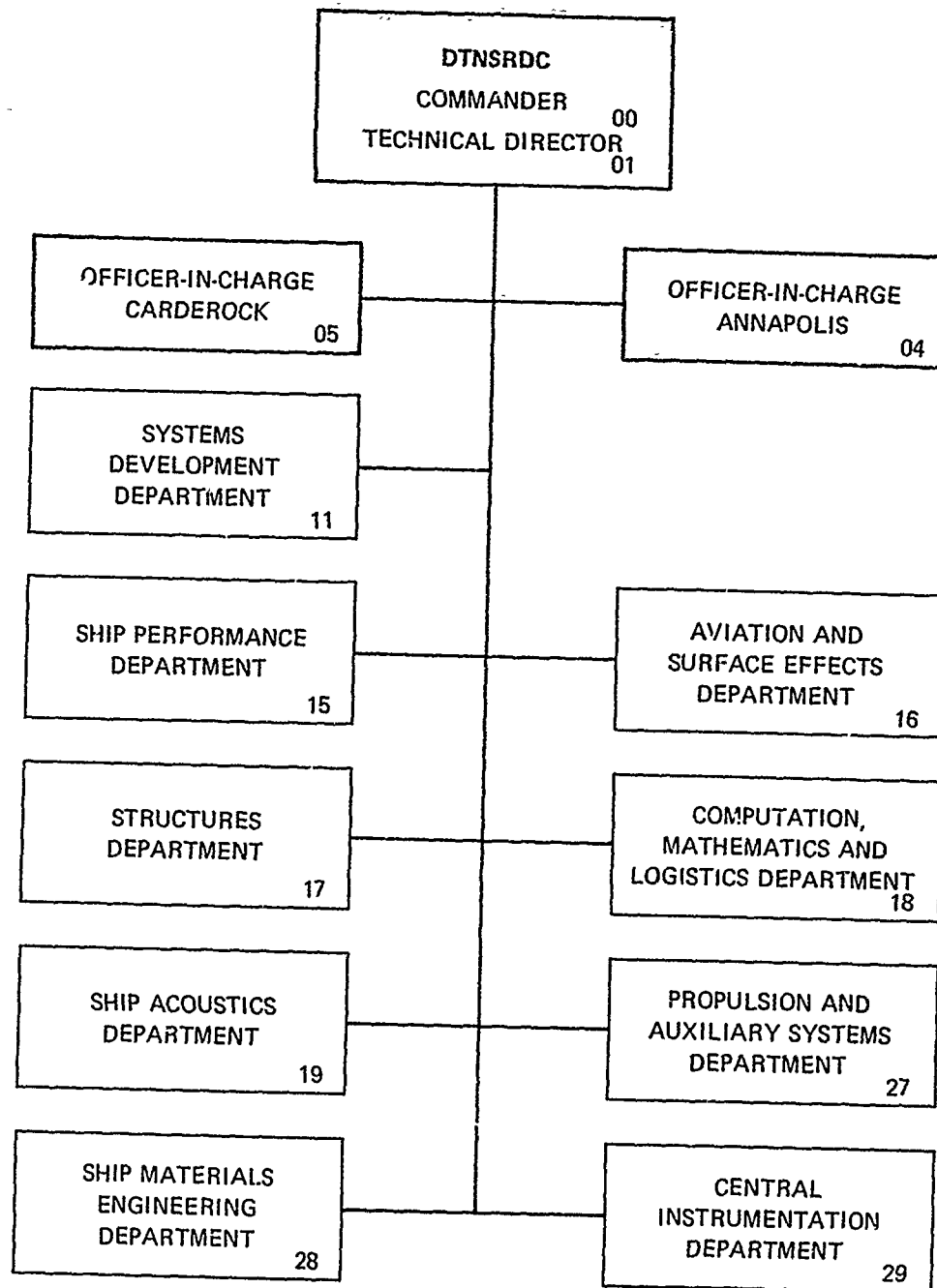
78 08 09 153

AD NO. _____
DDC FILE COPY

AD A 057 773

POWERING PREDICTION FOR SUR

MAJOR DTNSRDC ORGANIZATIONAL COMPONENTS



DTNSRDC ISSUES THREE TYPES OF REPORTS

- 1. DTNSRDC REPORTS, A FORMAL SERIES, CONTAIN INFORMATION OF PERMANENT TECHNICAL VALUE. THEY CARRY A CONSECUTIVE NUMERICAL IDENTIFICATION REGARDLESS OF THEIR CLASSIFICATION OR THE ORIGINATING DEPARTMENT.**
- 2. DEPARTMENTAL REPORTS, A SEMIFORMAL SERIES, CONTAIN INFORMATION OF A PRELIMINARY, TEMPORARY, OR PROPRIETARY NATURE OR OF LIMITED INTEREST OR SIGNIFICANCE. THEY CARRY A DEPARTMENTAL ALPHANUMERICAL IDENTIFICATION.**
- 3. TECHNICAL MEMORANDA, AN INFORMAL SERIES, CONTAIN TECHNICAL DOCUMENTATION OF LIMITED USE AND INTEREST. THEY ARE PRIMARILY WORKING PAPERS INTENDED FOR INTERNAL USE. THEY CARRY AN IDENTIFYING NUMBER WHICH INDICATES THEIR TYPE AND THE NUMERICAL CODE OF THE ORIGINATING DEPARTMENT. ANY DISTRIBUTION OUTSIDE DTNSRDC MUST BE APPROVED BY THE HEAD OF THE ORIGINATING DEPARTMENT ON A CASE-BY-CASE BASIS.**

UNCLASSIFIED

SECURITY CLASSIFICATION OF THIS PAGE (When Data Entered)

REPORT DOCUMENTATION PAGE		READ INSTRUCTIONS BEFORE COMPLETING FORM
1. REPORT NUMBER DTNSRDC-78/0621	2. GOVT ACCESSION NO.	3. RECIPIENT'S CATALOG NUMBER
4. TITLE (and Subtitle) POWERING PREDICTION FOR SURFACE EFFECT SHIPS BASED ON MODEL RESULTS.		5. TYPE OF REPORT & PERIOD COVERED
7. AUTHOR(s) R.A. Wilson, S.M. Wells and C.E. Heber		6. PERFORMING ORG. REPORT NUMBER Aero Report-1250
9. PERFORMING ORGANIZATION NAME AND ADDRESS David W. Taylor Naval Ship R&D Center Aviation and Surface Effects Department Bethesda, Maryland 20084		8. CONTRACT OR GRANT NUMBER(s)
11. CONTROLLING OFFICE NAME AND ADDRESS Naval Sea Systems Command Surface Effect Ships Project Office (PMS-304) Bethesda, Maryland 20084		10. PROGRAM ELEMENT, PROJECT, TASK AREA & WORK UNIT NUMBERS (See reverse side)
14. MONITORING AGENCY NAME & ADDRESS (if different from Controlling Office) Naval Sea Systems Command Surface Effect Ships Project Office (PMS-304) Bethesda, Maryland 20084		12. REPORT DATE July 1978
		13. NUMBER OF PAGES 15
		15. SECURITY CLASS. (of this report) UNCLASSIFIED
		15a. DECLASSIFICATION/DOWNGRADING SCHEDULE
16. DISTRIBUTION STATEMENT (of this Report) APPROVED FOR PUBLIC RELEASE: DISTRIBUTION UNLIMITED 16 SEP 82 14 50 30 3402		
17. DISTRIBUTION STATEMENT (of the abstract entered in Block 20, if different from Report)		
18. SUPPLEMENTARY NOTES Presented at the AIAA/SNAME Advanced Marine Vehicles Conference, San Diego, California, 17-19 April 1978. AIAA Paper No. 78-744.		
19. KEY WORDS (Continue on reverse side if necessary and identify by block number) Drag Drag Scaling Model Test Surface Effect Ship		
20. ABSTRACT (Continue on reverse side if necessary and identify by block number) A method employing the laws of dynamic similarity to scale experimental model data is presented for predicting the powering performance of large surface effect ships. The data are reduced to individual components, including cushion wavemaking drag, sidewall and appendage frictional and form drags, aerodynamic drag, and seal drag. These (Continued on reverse side)		

DD FORM 1 JAN 73 1473

EDITION OF 1 NOV 65 IS OBSOLETE
S/N 0102-LF-014-6601

UNCLASSIFIED

SECURITY CLASSIFICATION OF THIS PAGE (When Data Entered)

387025

TABLE OF CONTENTS

	Page
LIST OF FIGURES	iii
ABSTRACT.	1
INTRODUCTION.	1
COMPONENT DRAG DISCUSSION	1
WAVEMAKING DRAG	2
FRICTIONAL DRAG	4
AERODYNAMIC DRAG.	6
RESIDUAL DRAG	6
SCALING TECHNIQUE CORRELATION	8
REFERENCES.	9

LIST OF FIGURES

1 - SES Model During Powering Experiments	1
2 - Drag Component Breakdown for the SES-100B in State 1 Sea.	2
3 - Newman and Poole's Wave Resistance Parameter.	2
4 - Doctors' Wave Resistance Coefficient.	2
5 - A Comparison of Measured and Predicted Drag Variations with Pressure-to-Length Ratio.	3
6 - Seal Height Effects on Hump Traverse.	3
7 - Towing Tank Effects on Wave Resistance Coefficient.	3
8 - Predicted and Measured Unsteady Wave Resistance Coefficient at Near-Hump Speed.	4
9 - Predicted and Measured Unsteady Wave Resistance Coefficient at a Marginally Sub-critical Speed.	4
10 - Predicted and Measured Unsteady Wave Resistance Coefficient at a Marginally Super-critical Speed.	4

	Page
11 - Predicted and Measured Unsteady Wave Resistance Coefficient at a High Speed	4
12 - Sidewall Area Below the Chine A_{SW}	5
13 - Typical Sidewall Wetting.	5
14 - Percent Wetted Area for Low L/B SES	5
15 - Numerical Computation of Skin Friction Coefficient.	6
16 - Seal Loads Model.	7
17 - Seal Loads Model Components	7
18 - Seal Drag Scaling Factor Variation with Froude Number and Wave Height	8
19 - Correlation of SES-100B Data in a State 0 Sea	8
20 - Correlation of SES-100B Data in a State 1 Sea	8
21 - Correlation of SES-100B Data in a State 2 Sea	8

POWERING PREDICTION FOR SURFACE EFFECT SHIPS BASED ON MODEL RESULTS

Robert A. Wilson, Aerospace Engineer
Steven M. Wells, Aerospace Engineer
Charles E. Heber, Aerospace Engineer
Aviation and Surface Effects Department
David W. Taylor Naval Ship Research and Development Center
Bethesda, Maryland 20084

Abstract

A method employing the laws of dynamic similarity to scale experimental model data is presented for predicting the powering performance of large surface effect ships. The data are reduced to individual components, including cushion wavemaking drag, sidewall and appendage frictional and form drags, aerodynamic drag, and seal drag. These components are appropriately scaled by either Froude or Reynolds scaling laws. Water channel and model dimension effects on wavemaking drag are discussed and a technique for calculating sidewall wetted area is presented. An experimentally derived algorithm characterizing seal induced and frictional drag is explained. Drag predictions are compared with experimental trials data.

Introduction

The drag prediction technique presently used for scaling the model drag of a surface effect ship (SES) is different from that developed by Froude in that both the frictional and wavemaking drag terms can be accurately determined. The basic drag components are broken down into two classes: (1) those due to lift provided by the pressure region which dimensionally (or Froude) scale, and (2) those components which are due to friction and must account for skin friction coefficient changes with Reynolds number between the model and the prototype. The first theories¹ which were developed to describe the resistance characteristics of the SES broke the components into the wavemaking drag due to the pressure region and the frictional drag of the sidewalls. Seal drag estimates were based on early British expressions derived for hovercraft. SES technology has been significantly advanced since these early estimations were made. The various drag components have been studied extensively, largely through model experiments, and are now understood in much greater depth.

The resistance of an SES is usually estimated either from a theoretical approach (which has usually been correlated with or supplemented by experimental data) or one whereby experimentally derived model data are used extensively. The theoretical approach is used in parametric or sizing studies where one examines the effect of weight, length-to-beam ratio, or other parameters of a generalized design. These parametric prediction programs, however, may not be adequate to estimate the impact of the sometimes subtle physical differences between specific designs such as sidewall deadrise angle or chine effects, air-flow rate effects, or the inherent differences between planing or bag and finger seals. These design related differences can only be adequately evaluated through the use of model experiments and the analysis of the data. This paper summarizes a technique used by the Navy to calculate the resistance of a large prototype SES based on model test data.

The insight into understanding these components has involved many breakthroughs over the last decade. The ability

to measure the hydrodynamic forces on the seals in calm water as well as in seas has been a major advancement. The analysis of information contained in numerous model photographs such as the seal and sidewall wetting shown in the photograph of the SES-100A1 model in Fig. 1 has also been significant. Testing techniques and analysis procedures such as these have played a major role in the development of the SES.

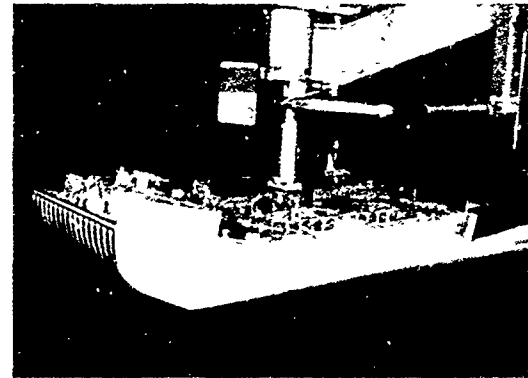


Fig. 1 - SES Model During Powering Experiments

Component Drag Discussion

The total drag D_T in the scaling program is broken down into components. The model aerodynamic drag component D_A is determined from specific model tare experiments. This tare value is later replaced by more appropriate wind tunnel results. The wavemaking drag D_W of the pressure region of the cushion is theoretically calculated. The frictional drag component D_f is determined through an accurate definition of the sidewall and appendage wetted areas. The component nominally referred to as the residual drag D_R is primarily comprised of the seal frictional and induced drag and the sidewall and appendage form drags.

Fig. 2 presents a breakdown of these components as drag-to-weight ratios for the SES-100B as a function of Froude number (based on cushion length) in a State 1 sea. This figure shows the residual (seal) drag dominating at subhump speeds, wavemaking drag dominating at or near the hump speed and frictional drag dominating at higher speeds. This component breakdown is typical for most designs but can be influenced by design variations such as the seals or the spray rails.

The drag components are broken into drag-to-weight ratio D/W values. The total drag is then viewed as follows:

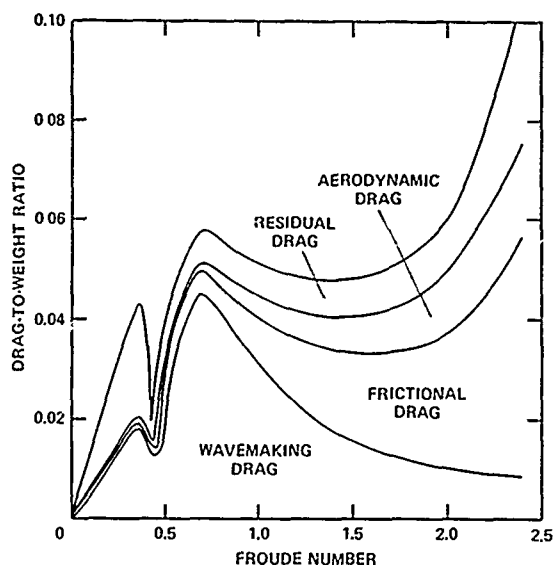


Fig. 2 - Drag Component Breakdown for the SES-100B in State 1 Sea

$$\frac{D_T}{W} = \frac{D_W}{W} + \frac{D_F}{W} + \frac{D_A}{W} + \frac{D_R}{W}$$

The following discussions in this paper deal with an understanding of these components and how they are scaled.

When working in model scale, one must understand dimensional scaling. The following table shows how the dimensions, forces, air-flow relations, and speeds of the model scale to prototype size according to Froude scaling:

Length - λ	Speed - $\lambda^{1/2}$
Area - λ^2	Pressure - λ
Volume - λ^3	Air Flow Rate - $\lambda^{2.5}$
Force - λ^3	Moments - λ^4

$$\lambda = \frac{(\text{Equivalent Cushion Length})_P}{(\text{Equivalent Cushion Length})_M}$$

The subscripts P and M denote prototype and model, respectively.

Wavemaking Drag

A vehicle moving through the water on a cushion of air generates waves due to the action of the pressure region on the water. This pressure region acts back on the vehicle to produce lift plus a wave drag component. Fig. 3 presents plots of the wave resistance parameter f_e as a function of Froude number for a family of length-to-beam ratio pressure regions as determined from Newman and Poole's theory.² Note that the cushion pressure and length are key parameters in calculating the wavemaking drag once the wavemaking resistance parameter is known. The adequacy of this wavemaking drag calculation has been demonstrated for the air cushion vehicle. Experimental investigations into the wavemaking drag of a hovercraft were made in England by Hogben^(3,4) and have been shown to agree with Newman and Poole's theoretical predictions in Reference 5. These experiments were conducted in such a manner that only the cushion acted on the water surface, no physical part of the

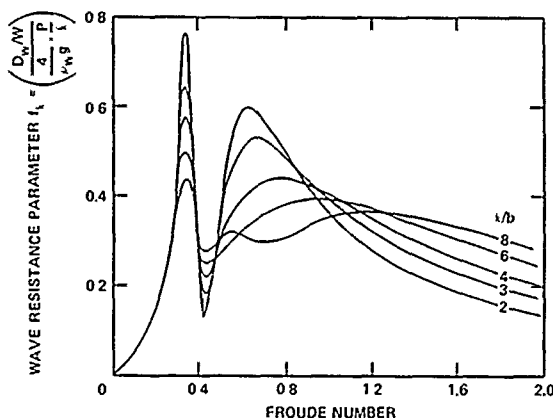


Fig. 3 - Newman and Poole's Wave Resistance Parameter

model touched the water surface. Since the SES has rigid side-walls and seals immersed in the water generating waves which interfere with the wave patterns generated by the pressurized field, the adequacy of the calculations again is questioned.

Model experiments were conducted to verify the use of Newman and Poole's predictions as well as to compare the experimental results with the wave resistance predictions of Doctors.⁶ Doctors' predictions have pressure fall-off parameters affecting the pressure region on the four sides. By varying these pressure fall-off parameters, the shape of the wave resistance characteristics with Froude number vary, predominantly in the subhump region. The results of the experiments⁷ showed that Doctors' predictions with pressure fall-off parameter values of $\alpha = 5.0$ and $\beta = \infty$ matched the subhump data. Thus, Doctors' wave resistance coefficient (Fig. 4) is used for calculating the wavemaking resistance for an SES.

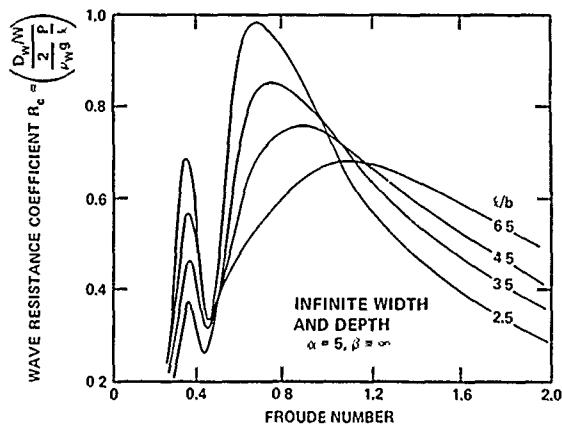


Fig. 4 - Doctors' Wave Resistance Coefficient

Because the cushion pressure is the key parameter in calculating the wavemaking drag and the wavemaking drag dominates in the hump region, the easiest way to verify wavemaking drag predictions is to vary the weight (and pressure) of the model and to compare the measured drag changes with predictions. This was done for the length-to-beam ratio 2.67 model and the results are shown in Fig. 5. This level of agreement demonstrates that the theory is adequate to predict this component for SES drag scaling. The spikes in the total

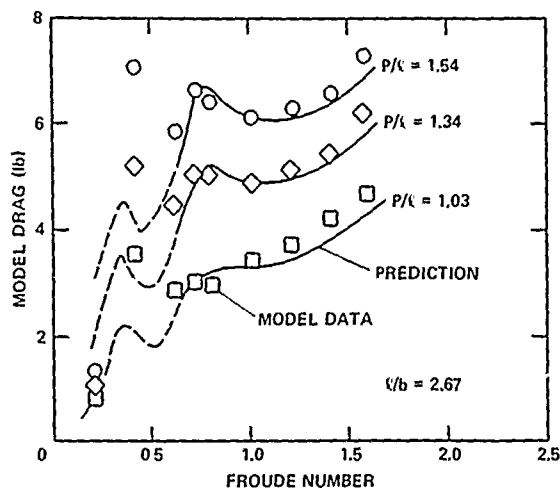


Fig. 5 - A Comparison of Measured and Predicted Drag Variations with Pressure-to-Length Ratio

resistance curve at the secondary hump (Froude number ≈ 0.4) are predominantly seal induced and can be lowered by raising the seals above the keel while traversing the secondary hump as shown by the model result in Fig. 6. When the seals are raised from their normal position $H_S = 0$, where the trailing edge of the seal is at the keel, to a value of $H_S = 0.36$, where the seal has been raised 36 percent of the cushion height above the keel, the subhump drag has been reduced by more than a factor of 3. When the seal is raised 18 percent ($H_S = 0.18$), the subhump and hump drag values are nearly the same. Note however in Fig. 6 that the lowest drag at the primary hump (Froude number ≈ 0.7) is with the seals located at the keel ($H_S = 0$).

The following equation presents the wavemaking drag-to-weight ratio calculation for both the model and the prototype which are the same.

$$\left(\frac{D_w}{W}\right)_M = R_c \left(\frac{P}{l}\right)_M \left(\frac{2}{\rho_w g}\right) = R_c \left(\frac{0.9 W}{b l^2}\right)_M \left(\frac{2}{\rho_w g}\right) = \left(\frac{D_w}{W}\right)_P$$

The value of the wave resistance coefficient R_c is determined from Fig. 4. The values of the beam b and length l of the cushion are determined from the model or prototype drawings and $0.9 W/b l^2$ replaces the pressure term. The above expression assumes that the water density of the model and the full-scale ships are the same. The water density must be properly accounted for both in determining the model weight and the model and prototype wavemaking drag values.

The size of the model and the dimensions of the towing tank must be properly scrutinized when interpreting model data. The wave resistance curves in Figs. 3 and 4 are for the pressure region passing over an infinitely deep and wide body of water. The restricted towing basin does not always represent such a body of water. Figs. 7 through 11 characterize the problems as shown by Doctors.* Fig. 7 shows the predicted steady-state wave resistance coefficient for a large model operating in a towing tank; the infinitely wide and deep case is shown for reference. The discontinuity for the finite tank case occurs at

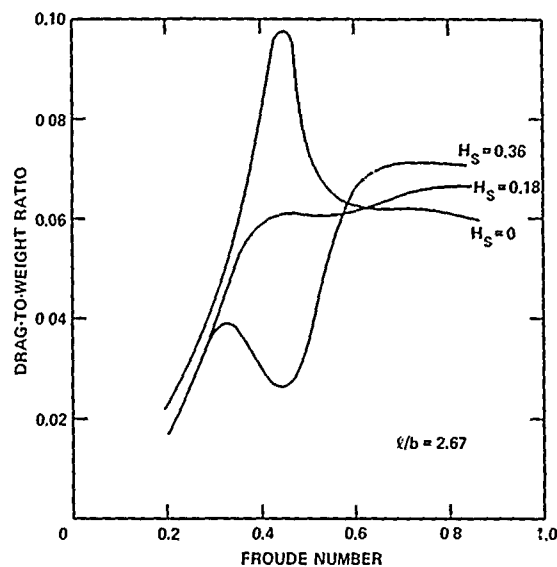


Fig. 6 - Seal Height Effects on Hump Traverse

the tank critical Froude number. The results of this figure show that substantial corrections in the wavemaking resistance may need to be made while testing in the restricted waters of the towing basin.

Doctors' unsteady wave resistance predictions have been verified by specific experiments at the David W. Taylor Naval Ship Research and Development Center. The results shown in Figs. 8 through 11 show the dependence of the wave resistance coefficient with nondimensional time in the restricted channel. Fig. 8 compares the predictions with experimental data at a near-hump speed while Figs. 9 and 10 show similar data at marginally subcritical ($F_l = 0.904$) and super-critical ($F_l = 1.00$) speeds. High speed experiments ($F_l = 1.80$) show no variation with nondimensional time as shown in Fig. 11.

The wavemaking resistance component calculated from Fig. 4 is then corrected using the appropriate steady or unsteady

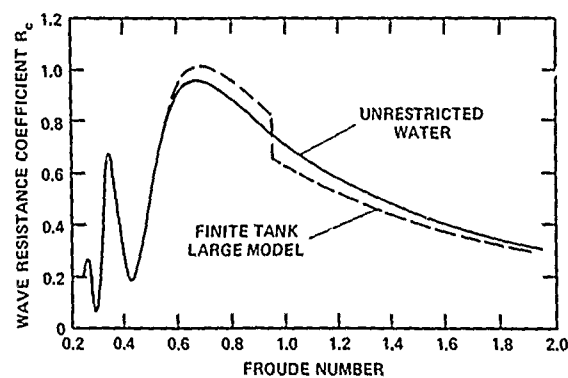


Fig. 7 - Towing Tank Effects on Wave Resistance Coefficient

*Documented in a formal DTNSRDC report by Lawrence J. Doctors entitled, "Unsteady Influences on a Surface Effect Ship Model in a Towing Basin."

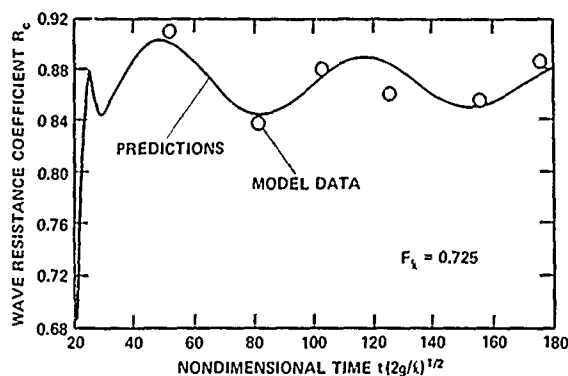


Fig. 8 - Predicted and Measured Unsteady Wave Resistance Coefficient at Near-Hump Speed

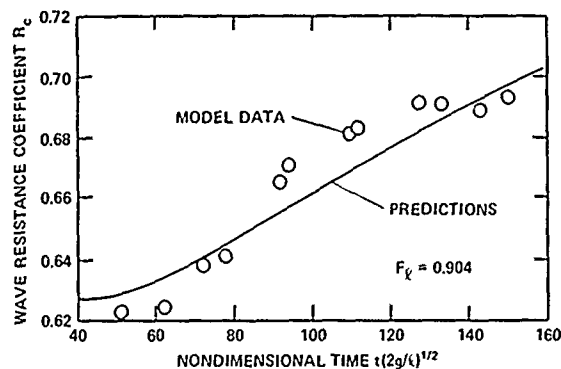


Fig. 9 - Predicted and Measured Unsteady Wave Resistance Coefficient at a Marginally Sub-critical Speed

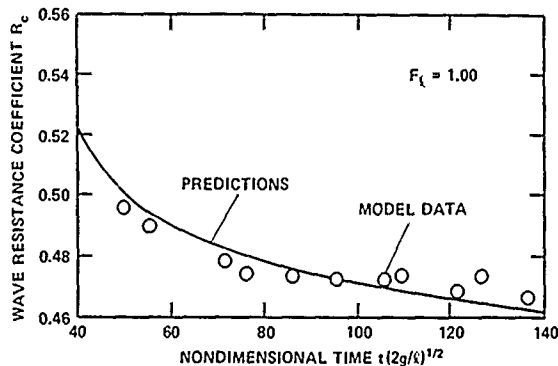


Fig. 10 - Predicted and Measured Unsteady Wave Resistance Coefficient at a Marginally Super-critical Speed

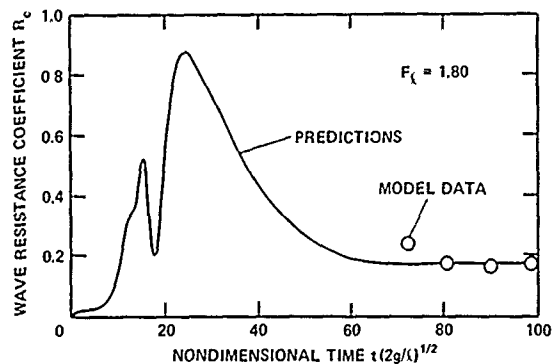


Fig. 11 - Predicted and Measured Unsteady Wave Resistance Coefficient at a High Speed

values of R_c for the specific model and towing facility. Since this is a time-dependent problem, the acceleration rate of the carriage and point in time when data are taken in the towing tank must also be considered.

Frictional Drag

The frictional drag component D_f is computed using the relationship

$$D_f = C_f \frac{\rho_w}{2} V^2 A$$

The two important considerations here are the values of the selected skin friction coefficient C_f and the wetted area A used in the calculation. The wetted areas scale as λ^2 as previously shown, and C_f varies with Reynolds number. The following discussion describes the technique used to determine the wetted area and the proper skin friction coefficients.

Previous techniques for computing the wetted areas on the sidewalls have assumed that model heave and trim angles as indicated from towing tank tests produce an accurate representation of the actual sidewall wetting. Photographs and movies from model tests however indicate that at posthump speeds, wetted areas determined from the heave and trim data are consistently smaller than the actual wetted areas observed. Using the photographs from many model tests, an empirically derived relationship between wetted area, trim angle, and Froude

number has been determined. The height of the chine or spray rail has been shown to have the greatest effect on wetted area. Therefore the projected sidewall area below the chine A_{SW} was used as a basis of comparison for determining sidewall wetting. The sidewall area A_{SW} is illustrated in Fig. 12 and is defined as the length of the sidewall at the keel times the average height of the spray rail or chine above the keel. The actual projected wetted area measured from test photographs A_{WET} was then expressed as a percentage of the sidewall area below the chine:

$$PRCNT = \frac{A_{WET}}{A_{SW}}$$

Typical sidewall wetting for an $L/B = 2.0$ SES at Froude numbers of 1.12 and 2.81 is illustrated in Fig. 13. The cases presented in Fig. 13 are for non-optimum trims.

The ratio of the actual sidewall wetted area to the area below the chine A_{WET}/A_{SW} is plotted in Fig. 14 as a function of Froude number for various trim angles. Curves of percent wetted area for various fixed trim angles of this typical case are shown, as well as an estimation of the percent wetting at optimum trim which varies with speed. The curves will vary with length-to-beam ratio, those in Fig. 14 were determined for a model with a length-to-beam ratio of 2.0.

The technique of determining the sidewall wetted area becomes a matter of interpolating a value of percent wetted area for the given L/B and trim angle. The projected wetted area

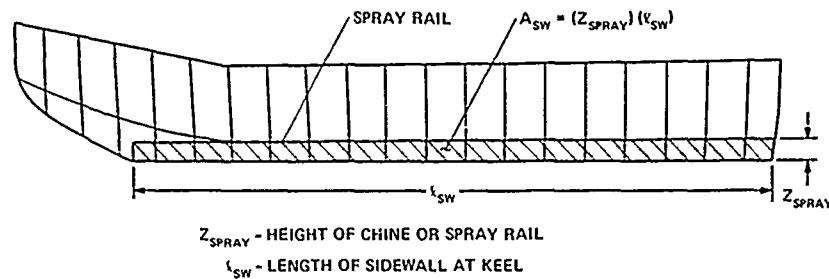


Fig. 12 - Sidewall Area Below the Chine A_{SW}

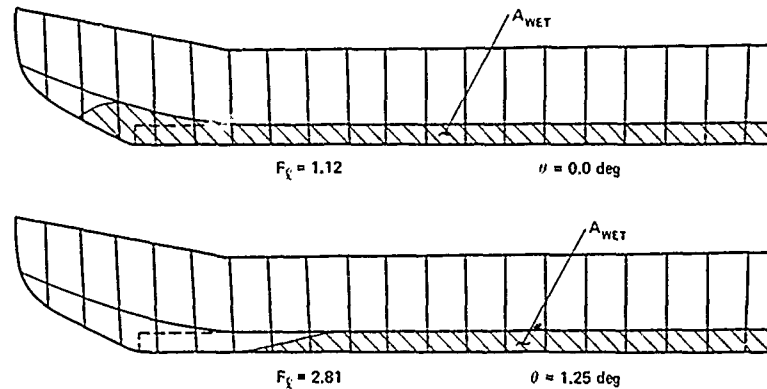


Fig. 13 - Typical Sidewall Wetting

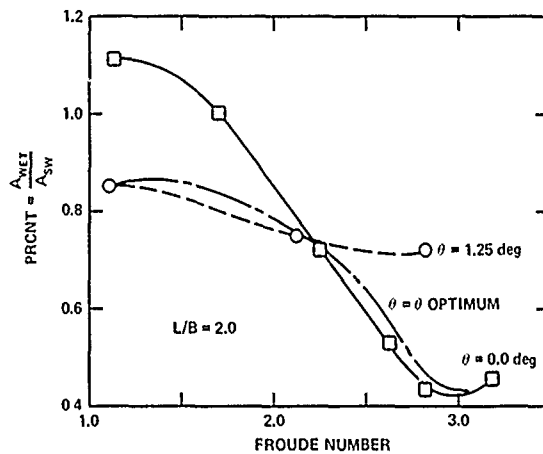


Fig. 14 - Percent Wetted Area for Low L/B SES

A_{WLT} is then calculated by multiplying the sidewall area below the chine A_{SW} by the percent wetting PRCNT.

$$A_{\text{WLT}} = (\text{PRCNT})(A_{\text{SW}})$$

Assuming a constant deadrise angle ϕ , the actual wetted area of the sidewall is determined by dividing the projected area by $\sin \phi$. The wetted area of any flat portions of the keel and the wetting on the cushion side of the sidewall are then added.

The inside wetting of the sidewalls at posthump speeds has been observed from photographs to be zero when the seals are

set at the keel. If the seals are set above the keel, the inside wetting is calculated using the area between the keel and a straight line connecting the lower tips of the bow and stern seals. This straight line approximation does not apply to subhump speeds, but because the frictional drag at these low speeds is small, the straight line approximation is still applicable.

The above discussion applies to the calculation of sidewall wetting in calm water. In rough water, additional area must be added to account for the wetting from waves. This additional area is equal to the corrected average waveheight $\bar{H}/2.5$ times the length of the sidewall and is added to the inside wetting. The outside of the sidewall is wetted to the spray rail or chine in calm water (see Fig. 13) and therefore, operation in waves generally does not increase the outside wetted area over that observed in calm water.

To complete the calculation of full-scale friction drag, the model and ship skin friction coefficients must be determined. The approach taken in the aircraft industry is used for the SES where surface roughness is evaluated (as opposed to that usually used by the ships community where the Schoenherr line is used with a ΔC_f added). The coefficient of friction is a function of Reynolds number and the equivalent sand roughness k_s of the sidewalls. Reynolds number is based on the sidewall length at the keel l_{SW} which is approximately the wetted length. The sand roughness is an equivalent measure of surface irregularities on the outer skin. Most model sidewalls have smooth painted surfaces and have shown (through the use of a profilometer) that their roughness is nominally 1 mil.

A roughness of nominally 1 mil is also considered to be close to the roughness anticipated for a large vessel. This value,

however, produces a value of C_f close to that determined from analysis of standard ship scaling techniques and substantiated with some full-scale data. Hoerner⁸ notes that the American Towing Tank Conference suggests that, due to ship roughness, a ΔC_f value of 0.0004 be added to the Schoenherr line C_{f0} . In the Reynolds number range in question for large SES vehicles, this happens to yield an effective roughness of approximately 1 mil. This value of C_f was obtained from studies of displacement ships in the 15-25 knot range. An interesting observation by Hoerner is that the ratio of C_f of the ship (including roughness effects) to C_{f0} , the value determined from the Schoenherr curve, increases as the speed capability increases. This fact seems reasonable when observing the C_f versus Reynolds number curves from Schlichting⁹. Schlichting shows that the slope of the smooth Schoenherr curve is always negative, whereas curves of constant ℓ/k_s values (characteristic length/roughness factor) become quite flat, and in some Reynolds number ranges, the slope is slightly positive. The comments made by Hoerner regarding this phenomenon were deduced from ship trials and seem to correlate quite well with the above-discussed C_f versus Reynolds number trend.

The value used for C_f can be determined from the following expressions for a wide range of vehicle sizes, roughness, and speeds. The first expression is the Prandtl-Schlichting derivation for the resistance of a smooth plate at zero incidence.

$$C_f = 0.455 (\log_{10} R_n)^{-2.58}$$

This equation corresponds to boundary layer flows that are turbulent and vary only as a function of Reynolds number. The second equation is derived for sand roughened plates and corresponds to a fully turbulent boundary layer.

$$C_f = \left(1.89 + 1.62 \log_{10} \left(\frac{\ell}{k_s} \right) \right)^{-2.5}$$

Both of these expressions are used, dependent on the Reynolds number and roughness. Fig. 15 presents the skin friction coefficient variation with Reynolds number for a roughness factor of 5×10^4 which is a typical value for a model. For low Reynolds numbers, such as are found on model appendages, sand separation strips should be used to assure turbulent flow. Model experiments of the sidewalls tested with and without sand separation strips show that the sidewalls are always in turbulent flow.

This discussion described how the skin friction coefficients and wetted areas for both the model and the prototype are determined. Thus, the relationships between model and prototype frictional drag-to-weight ratios is as follows:

$$\left(\frac{D_f}{W} \right)_P = \left(\frac{D_f}{W} \right)_M \left(\frac{C_{fP}}{C_{fM}} \right)$$

Some typical 1 mil skin friction coefficient values are as follows.

Size	C_f
1/30-scale 3KSES Model	0.0033
1/20-scale 3KSES Model	0.0030
100-Ton Testcraft	0.0024
3KSES Prototype	0.00195

Appendage frictional drag is calculated in a manner similar to the sidewall frictional drag. Wetted areas can be determined from drawings.

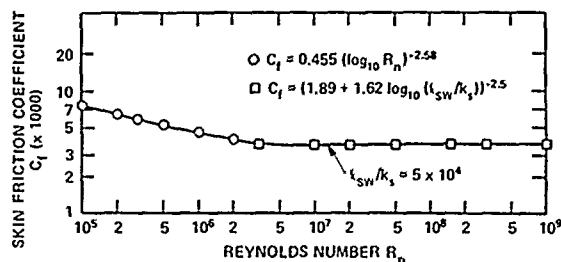


Fig. 15 - Numerical Computation of Skin Friction Coefficient

Aerodynamic Drag

Hydrodynamic models poorly represent the aerodynamics of the prototype design. As shown in Fig. 1, the models normally do not have weather decks or superstructures. The local aerodynamic flows present near the model in the towing tank are similar neither in magnitude nor in direction to those expected in the open water due to boundary layer differences and channel and carriage flow disturbances. Reynolds number effects also must be considered. Because of these differences, the aerodynamic forces on the hydrodynamic model are measured as tare using special test techniques. This model tare value for drag is subtracted from the measured model drag leaving only the hydrodynamic drag components. During the course of scaling the individual drag components, wind tunnel data for the appropriate configuration is substituted.

The equation used to calculate the aerodynamic drag D_A of the prototype is:

$$D_A = C_{D_a} \frac{\rho_a}{2} V^2 A_f$$

where C_{D_a} is the aerodynamic drag coefficient. The reference area A_f is determined as the product of the overall beam and the height from the water to the weather deck. The aerodynamic drag coefficient can vary from 0.3 for a clean hull with no superstructure to 1.1 for a square design with a "dirty" superstructure. If no aerodynamic drag coefficient is available, a value of $C_{D_a} = 0.5$ can be used for a reasonably designed craft.

Residual Drag

Residual drag D_R is the drag component remaining after subtracting the previously described components from the total model drag. In terms of drag-to-weight ratio, this becomes

$$\frac{D_R}{W} = \frac{D_T}{W} - \frac{D_f}{W} - \frac{D_w}{W} - \frac{D_A}{W}$$

The residual drag component is predominantly comprised of the momentum drag, sidewall and appendage form drag, and seal drag. The momentum and form drags are relatively small quantities; the seal drag term represents the major portion of the residual drag term.

The momentum drag occurs when the constant mass flow entering from the fans into the cushion is brought from a particular velocity to zero velocity relative to the craft. In addition, a cushion thrust is produced by the flow exiting under the stern seal. The magnitudes of these two forces are equal within experimental accuracy, and because the forces are opposing, the sum of the momentum drag and cushion thrust are assumed to be zero.

The sidewall and appendage form and pressure drag terms D_p are small but not negligible. Both can be computed using simple techniques. For both, the form drag is equal to the submerged cross-sectional area multiplied by the average head of water displaced. This computational technique works very well for the sidewalls. The appendages may require a correctional term to account for appendage shaping. This, however, can be done on a case-to-case basis. Both the sidewall and appendage form drags D_p are Froude scaled.

The remainder and the larger portion of the residual drag term, then, is predominantly seal drag. Scaling seal drag involves the breakdown of seal drag into seal frictional and seal induced drag components. These components, once determined, then must be scaled independently.

The determination of the magnitude of the seal forces is described in two reports.* These reports describe the testing of an SES model, segmented and instrumented to isolate the loads acting on the bow and stern seal. Figs. 16 and 17 show a set-up photograph and a schematic of the model as tested. As shown, the model consisted of three segments. One was the bow seal module, which contained the bow seal, a small portion of the wetdeck and a short portion of the sidewall. The second module was the centerbody and stern seal module which comprised the bulk of the wetdeck and to which the stern seal was attached. The third module was the sidewall support module which held the bulk of the sidewall. The three modules were attached to each other by means of two balances, yielding measured forces as shown in the schematic. Three different seal designs were tested in both calm and rough water. The bow seal designs consisted of a planing seal, a finger seal, and a bag and finger seal. The raw data from the tests yielded total forces acting on the bow and stern seals due to cushion pressure and aerodynamic and hydrodynamic influences. The model was instrumented in such a way as to allow the extraction of the total hydrodynamic seal drag (equivalent to the total seal drag being discussed here).

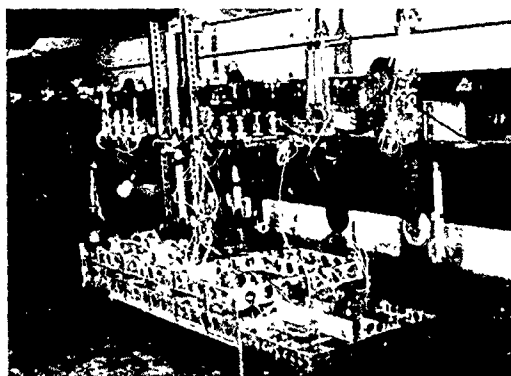


Fig. 16 - Seal Loads Model

Knowing the total seal drag, the model operating conditions from the above tests, and the bow and stern seal attitudes, it was then possible to calculate the amount of total seal drag due to frictional effects. The difference between the total seal drag and the frictional seal drag is the seal induced drag. These calculations were carried out for a planing type bow seal configuration for a variety of velocities and sea conditions. Fig. 18 shows how the seal drag scaling factor K_1 varies with ship Froude number for various sea conditions as determined from the seal experiments. The factor K_1 is the ratio of the seal induced drag D_{S1} to the seal total drag D_{ST} . The figure shows that there is a noticeable dependency of K_1 on Froude number

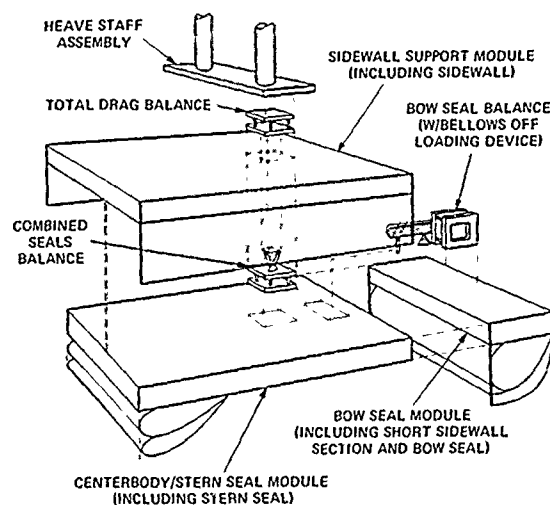


Fig. 17a - Seal Loads Model Schematic

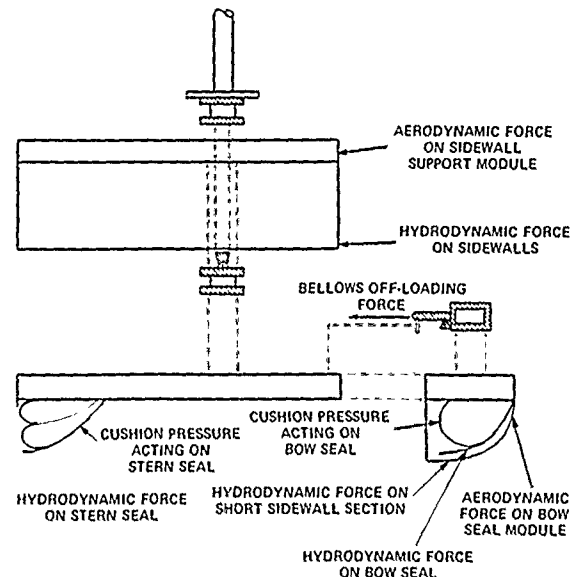


Fig. 17b - Seal Loads Model Forces

Fig. 17 - Seal Loads Model Components

*Documented in two DTNSRDC reports by C E Heber entitled "An Analysis of Seal Loads and Their Effect on the Performance of a Surface Effect Ship in Calm Water" and "An Analysis of Seal Loads and Their Effect on the Performance of a Surface Effect Ship in Rough Water."

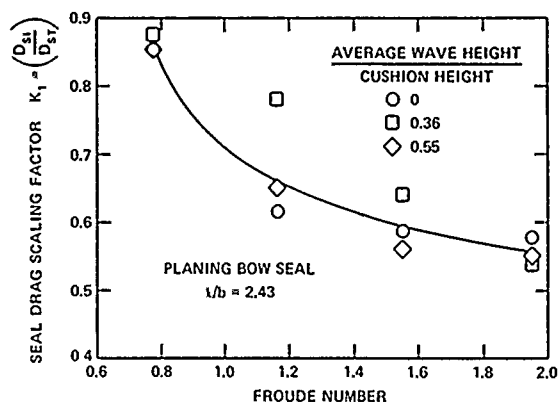


Fig. 18 - Seal Drag Scaling Factor Variation with Froude Number and Wave Height

(or speed). However, the data generally collapse with respect to wave height variations. Although overall drag increases occur with sea state, the relative amounts of induced and frictional drag remain constant at particular velocities. Similar data exist for other seal types (finger, and bag and finger configurations) but are not presented here.

At present, expressions are being developed to accurately predict seal drag for the various seal designs previously described. When this is completed, residual drag (in the true sense of the word) will be very small and handled separately from the seal drag. However, at the present time residual drag is scaled as follows.*

$$\left(\frac{D_R}{W}\right)_P = \left(\frac{D_P}{W}\right)_M + \left[K_1 + (1 - K_1) \left(\frac{C_{fP}}{C_{fM}} \right) \right] \left(\frac{D_{ST}}{W} \right)_M$$

This expression separates the seal drag into its two components by virtue of the K_1 term. Then, that part corresponding to frictional drag $(1 - K_1)$ is scaled utilizing Reynolds scaling; that part corresponding to the induced drag K_1 is Froude scaled as is the sidewall and appendage form and pressure drag.

Scaling Technique Correlation

The technique discussed in this paper has been used to compare scaled model data with full-scale trials data from the SES-100B. The SES-100B trials were conducted similar to model experiments, evaluating the effects of weight, longitudinal center-of-gravity location, air flow rate, and sea state. The model experiments in seas were run in the same scaled stationary wave spectrum measured during the trials program. The data are presented in Fig.

presented in Figs. 19 through 21 for State 0, 1, and 2 seas, respectively. The solid line is the scaled, faired model data while the data points are trials data. The data are presented in terms of drag-to-weight ratios because the trials data apply to varying weights due to fuel burnoff. These three figures show the adequacy of the scaling technique.

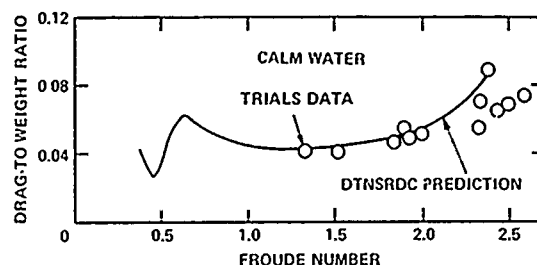


Fig. 19 - Correlation of SES-100B Data in a State 0 Sea

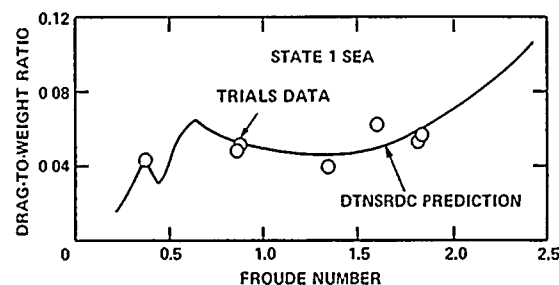


Fig. 20 - Correlation of SES-100B Data in a State 1 Sea

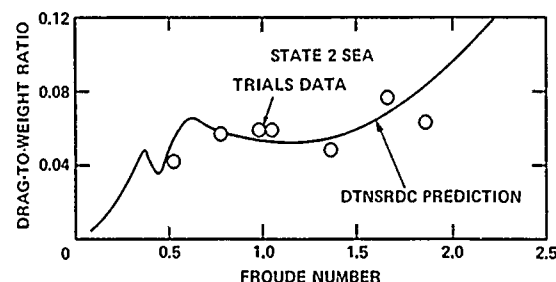


Fig. 21 - Correlation of SES-100B Data in a State 2 Sea

As further data become available, trials data from the SES-100A with modified seals and sidewalls will be compared to scaled model data to further verify the scaling technique. In addition, data from the XR-5 trials will be compared to scaled model data to verify the scaling routines relative to higher length-to-beam ratio surface effect ship designs.

*Documented in a DTNSRDC report by S.M. Wells entitled "Residual Drag Scaling of a Surface Effect Ship Model in Sea State 6 at Near-Hump Speeds."

References

1. Ford, A.G., "Progress in Air Cushion Vehicles," David Taylor Model Basin Report 2280 (Oct 1966).
2. Newman, J.N. and F.A. Poole, "The Wave Resistance of a Moving Pressure Distribution in a Canal," David Taylor Model Basin Report 1619 (Mar 1962).
3. Hogben, N., "Research on Hovercraft Over Calm Water," Royal Institute of Naval Architects, Vol. 109, No. 3 (Jul 1967).
4. Hogben, N., "An Investigation of Hovercraft Wave-making," Journal of the Royal Aeronautical Society, Vol. 70, No. 662 (Feb 1966).
5. Williams, R.M., "Study of the Wavemaking of Captured Air Bubble Vehicles," Virginia Polytechnic Institute, Engineering Mechanics Department Report (Mar 1968).
6. Doctors, L.J., "The Wave Resistance of An Air-Cushion Vehicle," University of Michigan (Dec 1970).
7. Van Dyck, R.L., "Hump and Sub-Hump Performance Tests of a Surface Effect Ship, Phase I - Deep and Shallow Water Tests," Stevens Institute of Technology, Letter Report SIT-DL-72-1592 (Apr 1972).
8. Hoerner, S.F., "Fluid-Dynamic Drag," 1965 Edition, Published by the Author, Midland Park, New Jersey (1958).
9. Schlichting, H., "Boundary Layer Theory," Sixth Edition, McGraw-Hill Book Company, New York, N.Y. (1968).

INITIAL DISTRIBUTION

Copies

1 ARPA/Library
 1 CHONR/461
 1 ONR SCI LIAISON GP/APO
 1 NAV STRATEGIC SYS PROJ
 OFFICE
 PM-1
 1 USNA/Library
 2 NAVPGSCOL
 1 Library
 1 D. Layton/Aero Dept
 1 NROTC & NAVADMINU, MIT
 1 NSWC/Dahlgren
 Tech Library
 1 NSWC/White Oak
 Tech Library
 1 NUSC/Tech Library
 19 NAVSEA
 1 SEA 03B
 1 SEA 032
 1 SEA 09G32
 16 PMS-304-141
 1 NISC
 3 NAVSEC
 1 SEC 6110
 1 SEC 6114
 1 SEC 6136
 12 DDC
 1 Coast Guard HQ
 Library/5-2

Copies

1 Marine Corps HQ/AX
 A.L. Slafkosky/Sci
 Advisor
 2 Maritime Admin
 1 R&D Office
 1 Div of Ship Design
 1 Library of Congress
 Science & Tech Div
 1 AIAA/D. Staiger
 1 SIT/Davidson Lab
 J.P. Breslin

CENTER DISTRIBUTION

Copies

Code	Name
5214.1	Reports Distribution
522.1	Library (C)
522.2	Library (A)
522.3	Aerodynamics Library